Labor & Engenho

Evaluation of the Effect of Curing Conditions on Compressive Strength and Microstructure of Alkali-Activated Binders

DOI: 10.20396/labore.v18i00.8676085

Marília Lima Tavares
https://orcid.org/0009-0003-6934-6130
Universidade Federal do Ceará / Crateús [CE] Brasil

Daniel Lira Lopes Targino
https://orcid.org/0000-0003-2226-7868
Université Gustave Eiffel / Nantes [França]

Antonio Eduardo Bezerra Cabral
https://orcid.org/0000-0001-6394-1164
Universidade Federal do Ceará / Fortaleza [CE] Brasil

Heloina Nogueira da Costa
https://orcid.org/0000-0001-9960-2383
Universidade Federal do Ceará / Crateús [CE] Brasil

ABSTRACT

Alkali-activated binders (AABs) are a trending subject in research as a sustainable alternative to ordinary Portland cement (OPC). In recent years, there has been an increased interest in the development of AAB composites and fabrication methods. Their properties are greatly influenced by temperature, humidity, formulations and constituent types. Therefore, it is essential to understand these factors to obtain adequacy to use. This article evaluates the effect of (i) temperature, in ambient (25°C) and thermal (50°C for 24 hours) curing, (ii) exposure to air – either isolated or in contact with the air atmosphere – and (iii) susceptible to external humidity – such as air contacted or submerged – as curing conditions for the fabrication of AAB. The evaluation included compressive strength tests at 1, 28, 63, and 91 days, along with microstructural evaluation through morphology analysis and incidence of voids. Digital image processing (DIP) was carried out using ImageJ software. The proposed AAB consisted of fly ash (FA) and steel slag from the Basic Oxygen Furnace (BOF) process as precursors, with sodium hydroxide (NaOH) and sodium silicate ($NaSi_2O_3$) as alkali activators, applied in mortar production. The results of compressive strength revealed that mortar subjected to thermal curing, isolated from air contact and external humidity, exhibited the highest outcome, with 46.05 MPa. Microstructural analysis indicated the formation of hydrated aluminosilicate gels and the presence of voids, including partially reacted particles and microcracks. The DIP analysis of the sectional area demonstrated that void incidence under 50 μm^2 predominantly did not affect compressive strength.

KEYWORDS

Alkali-Activated Materials. Fly Ash. BOF Slag. Curing Conditions.

Submetido 17 mar 2024 / Aceito 18 jul 2024 / Publicado 18 set 2024

1. Introduction

In Brazil, in 2022, a total of 62.7 million tons of ordinary Portland cement (OPC) were consumed (National Cement Industries Syndicate, 2023), with high greenhouse gas emissions (GHGe), along with an expressive natural resources' consumption. The production of 1 ton of OPC releases between 0.6 and 1 ton of GHGe (Monteiro *et al.,* 2017; Zhang *et al.*, 2018; Mian, 2013).

The demand for more sustainable solutions, with lower environmental impact has been on the rise in recent years. In this context, alkali-activated binders (AABs) are alternatives to OPC with improved sustainability. AABs derive from the combination of a powder precursor, rich in aluminum (SiO_2) and silicates (Al_2O_3), and alkaline activators, in a high-pH aspect (Provis, 2018).

Precursors with high calcium content favor the AAB formation with higher hydrated calcium aluminosilicate gel (C-A-S-H) (Provis, 2014; Bernal *et al.*, 2014). Similarly, precursors rich in SiO_2 and Al_2O_3, without high calcium content, constitute hydrated sodium aluminosilicate gels (N-A-S-H) with amorphous phases (Langaro, 2016).

Different materials can serve as precursors and industrial by-products or wastes also present a high content of aluminosilicates, being feasible for those applications. Their usage contributes to reducing waste disposal in the environment and lowering natural resource usage (Provis & Van Deventer, 2014; Silva *et al.,* 2017). AAB production results in lower GHGe due to the absence of calcination. The production of AABs, compared to OPC, leads to a reduction of up to 80% in GHGe, depending on the composition (Duxson *et al.,* 2007).

AAB composites exhibit mechanical properties similar to OPC (Azevedo, 2017; Juenger, 2011; Langaro, 2016). It is important to note that several factors can affect the properties of Alkali-activated binders (AABs), including the chemical composition of the precursors' materials, binder mixing design, and curing conditions.

Thermal curing at temperatures ranging from 50°C to 60°C is often addressed for AABs (Bakria *et al.,* 2011; Nath *et al.*, 2016). It helps to speed up the chemical reactions, increases the compressive strength, and reduces the setting time (Criado *et al.*, 2010). Thermal curing can be carried out at temperatures between 40°C and 100°C (Rai *et al.,* 2018).

The temperature affects the curing conditions, having also influences the chemical composition, particle size, and amorphism degree and chemical phases of the precursors (Sathonsaowaphak *et al.,* 2009; Komljenović *et al.*, 2010; Chindaprasirt *et al.*, 2012). The literature presents results that indicate that thermal curing has negative effects on strength, attributed to microcracks formation in the binder matrix (Gebregziabiher *et al.*, 2016, Husein *et al.,* 2016).

Additionally, exposure to water or atmospheric air during curing can influence the AAB formation. When samples are exposed to air in an unsaturated environment, water evaporation occurs, leading to a reduction in alkaline solution and increased salt precipitation in the pores, as an efflorescence effect (Izquierdo *et al.*, 2010). The samples' isolation from atmospheric air is recommended to maintain the same water availability while hardening (Criado *et al.*, 2010).

However, it is not advisable to use water immersion curing for low-calcium AABs as it can dissolve the reaction activator and reduce the material's strength development (Provis, 2018). The influence of these curing condition parameters remains a gap in the study of AABs. This understanding is essential for the development of more suitable composites, quantifying these variables' impact on aspects of compressive strength and microstructure formation.

This article evaluates the impact of different curing conditions on alkali-activated binders (AABs) applied to mortars. The study encompasses (i) the temperature variation, such as ambient curing at 25°C and thermal curing at 50°C for 24 hours, (ii) air exposure, such as isolated or exposed to the air, and (iii) interaction with external humidity, such as with or without interaction with external humidity. The analysis includes compressive strength tests at 1, 28, 63, and 91 days and microstructural analysis, assessing morphology, pores incidence, and void content for 28 days.

The proposed AAB is a binary mixture of Fly Ash (FA) and Basic Oxygen Furnace (BOF) steel slag as precursors. This binder has been previously studied by Costa (2022), Caetano (2021), and Araújo (2022) with temperature variations. It is intended to deeply understand their influence and explore their influence on the

outcomes.

2. Materials and methods

2.1. Materials

The proposed AABs consist of FA class F (with total content of Si, Al and Fe oxides equal to 80.93%), according to ASTM C618:2019, and steel slag derived from a Basic Oxygen Furnace (BOF) process as precursors. A binary mixture of sodium hydroxide (NaOH) and sodium silicate (Na_2SiO_3) was adopted as alkaline activators. This AAB was applied in mortars with the addition of natural fine aggregate. Chemical composition through X-ray fluorescence (XRF) analysis for the precursors is presented in Table 1.

Table 1. Chemical composition of precursors in mass percentage (wt%). Source: Araújo (2022); Targino *et al.* (2024).

	Al_2O_3	**SiO_2**	P_2O_5	SO_3	Cl	K_2O	**CaO**	TiO_2	MnO	Fe_2O_3	ZnO	SrO
FA (wt%)	**11.14**	**42.20**	0.53	1.08	0.05	3.91	**10.30**	2.74	0.27	26.98	0.15	0.65
BOF (wt%)	**1.94**	**5.64**	0.84	0.86	0.04	0.14	**53.11**	-	2.97	34.40	0.06	-

The specific mass was determined according to NBR 16605 (ABNT, 2017), obtaining the results of 2.34 g/cm³ for FA and 3.13 g/cm³ for BOF. The specific surface area was obtained according to NBR 16372 (ABNT, 2015), achieving 4790 cm²/g and 3360 cm²/g, respectively.

Sodium hydroxide in flake form with a purity of 97.9%, was utilized. The solution was prepared 24 hours in advance using with a molar concentration of 8 mol/L. The sodium silicate solution used has a 2.21 SiO_2/Na_2O ratio (silica modulus) and a specific mass of 1.58 g/cm³.

Natural sand was used, with a specific mass of 2.63 g/cm³ and bulk density of 1.56 g/cm³, determined according to DNER ME 194 (DNER, 1998) and NBR 16972 (ABNT, 2021), respectively. The pulverulent content was found 2.94%, according to NBR 16973 (ABNT, 2021), with a 2.36 mm maximum diameter size and fineness modulus of 2.44, as per NBR 17054 (ABNT, 2022).

The mortar was produced in the mass proportion ratio of 1 : 2.66 : 0.6 (precursor: sand: activator). The precursor was composed of 50% FA and 50% BOF, and the activator 50% sodium hydroxide and 50% sodium silicate, all in mass proportion, based on the work of Costa (2022) and Targino *et al.* (2024). The total silica modulus was 1.40, and the alkali content was 10%, according to the recommended range of 5 to 15% from the literature (Soutos *et al.*, 2016; Thomas & Peethamparan, 2017; Ding *et al.*, 2018).

The mixing procedure was conducted using a planetary mixer. Initially, precursors were homogenized, followed by a gradual addition of the activators. For the last, natural sand was added and the planetary mixer was activated at low speed (62±5 rpm) for 1 minute and 30 seconds. A 1-minute pause was taken to verify homogeneity. Finally, the planetary mixer was reactivated at low speed for another 1 minute and 30 seconds. Figure 1 illustrates the aspect of the consistency table test.

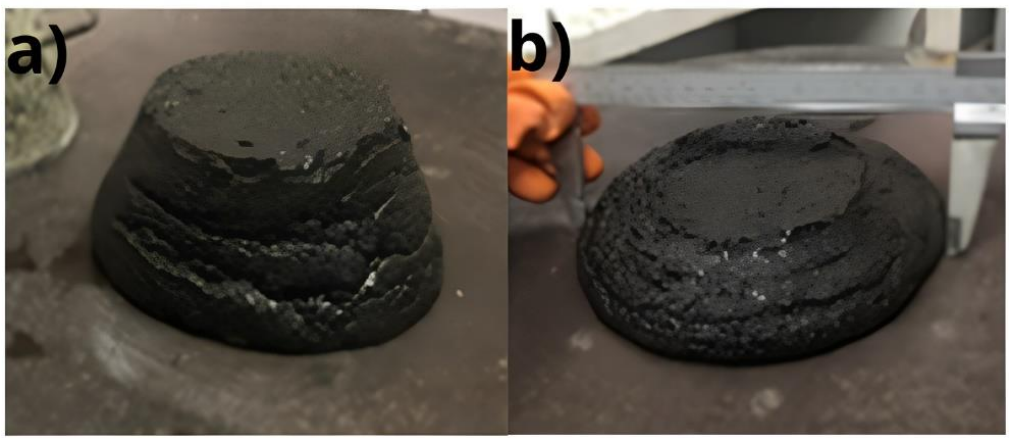

Figure 1. The visual aspect of the Consistency Table Test (a) on the initial molding and (b) after testing on the diametral measures.

The mortar exhibited a plastic consistency visual aspect, indicated by the average spread diameter of 199.3 mm from the flow table test result, according to NBR 13276 (ABNT, 2016).

The mortars were subjected to three different curing conditions, (i) temperature, (ii) atmospheric air exposure, and (iii) interaction with external humidity, in a disposal of 6 combinations. They were evaluated for compressive strength at 1, 28, 63, and 91 days. Table 1 provides detailed information on the curing conditions adopted in this study.

Table 2. Disposition of the Curing Conditions combined

Conditions Labels	Temperature (ºC)	Air Exposure	External Humidity
ASN1	Ambient (25°C)	Sealed	Not Exposed
AEA2	Ambient (25°C)	Exposed	Air Exposed
ASS3	Ambient (25°C)	Sealed	Submerged
TSN4	Thermal (50°C/24h)	Sealed	Not Exposed
TEA5	Thermal (50°C/24h)	Exposed	Air Exposed
TSS6	Thermal (50°C/24h)	Sealed	Submerged

The thermal curing was conducted in the first 24 hours after molding in an oven at 50°C. After that period, the specimens were kept at an ambient temperature (25°C). The specimens not exposed to air and external humidity were wrapped in polypropylene film after demolding. The film was maintained up to the testing ages. Specimens exposed to air and external humidity were stored in ambient conditions, while those submerged were stored underwater with ambient temperature.

2.2 Experimental Program

The compressive strength test was conducted on cubic specimens with 4 cm edges, according to NBR 13279 (ABNT, 2005). Statistical analysis was performed using Analysis of Variance (ANOVA), and the means were analyzed using Tukey's test on the compressive strength outcomes over time.

For the microstructure analysis, specimens from three curing conditions were selected: ambient curing with air exposure (AEA2), thermal curing with air isolation (TSN4), and thermal curing submerged (TSS6). The selection of conditions was based on the curing conditions and the compressive strength results. The samples were collected from fragments of the compressive strength-tested specimens at 28 days.

Scanning Electron Microscopy (SEM) was employed for microstructure analysis, utilizing the Quanta 450-FEG – FEI microscope in SE mode (surface image) at magnifications of 2.500X and 10.000X. Aspects of morphology and void content were analyzed. Additionally, void distribution analysis was conducted through digital image processing using the *ImageJ* software. The SEM images were binarized to distinguish the solid structure from the voids, determining the surface area of the void content (SUN *et al.*, 2022).

4. Results and discussion

4.1 Compressive Strength Analysis

The influence of the curing conditions assessed on the compressive strength of the mortars is presented in Figure 2.

Compressive strength after 1 day casting was significantly higher for mortars subjected to thermal curing. On those, the highest strength was 42.93 MPa for the TEA5 subjected to thermal curing, air exposure and interaction with the external humidity. Formulation at ambient temperature presented values ranging from 1.5 to 6.7 MPa.

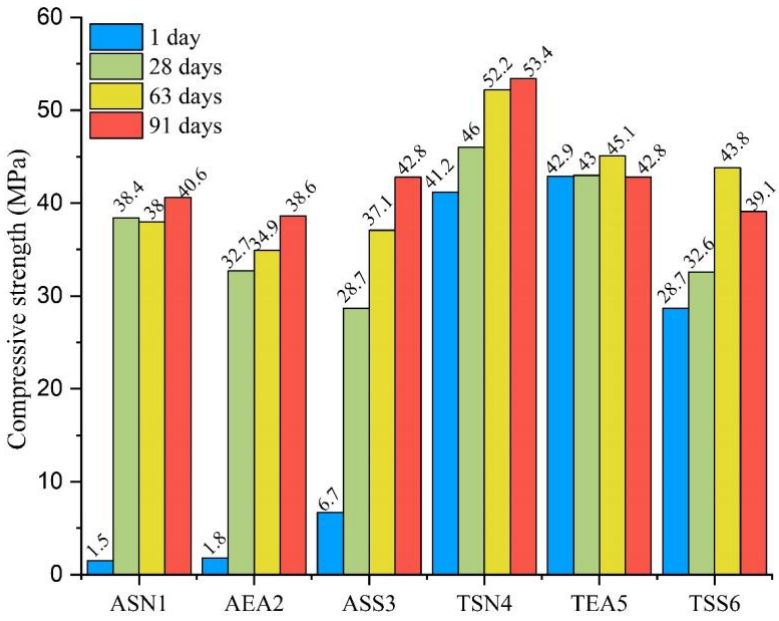

Figure 2. Compressive Strength at 1, 28, 63 and 91 days

In the first 24 hours, temperature curing was demonstrated to be a predominant factor for rapid strength evolution, which is consistent with the literature (Gómez-Casero *et al.,* 2021). Also, air exposure and external humidity interaction resulted in no meaningful difference in ASN1 and AEA2 at ambient curing. The same was observed in TSN4 and TEA5, both with thermal curing.

Mortars under conditions ASS3 and TSS6, at ambient temperature and thermal curing, respectively, were submerged in water for an additional 24 hours before rupture. Therefore, they were tested 48 hours after molding and 24 hours after submerged curing, as the paste was not completely cured during the first 24 hours. Therefore, they were tested 48 hours after molding and 24 hours after submerged curing. The results show contrasting effects of submerged curing, as when kept at room temperature and exposed in the first 24 hours, submerged curing increased the strength compared to other samples at room temperature (ASN1 and AEA2). However, the time difference should also be considered, as ASS3 was broken 24 hours after ASN1 and AEA2. Regarding the TSS6 sample, submerged curing led to a decrease in strength when compared to TSN4 and TEA5, both cured at 50°C.

At 28 days, the mortar subjected to the TSN4 condition (thermal curing at 50°C for 24 hours, with the specimen isolated from air exposure and interaction with air humidity) achieved the highest result, with an average value of 46.05 MPa, while the lowest result was observed for the exposure to the ASS3 condition, with 28.7 MPa.

At 28 days, it is evident that there was an increase in strength in samples subjected to all curing conditions compared to the earlier age. This is observed in similar studies addressing the increase in strength over time, having the most expressive strength evolution for the 1 to 28 aging days (Zhang *et al.,* 2018). Chindaprasirt *et al.* (2010) studied the properties of AAB mortars produced with a high content of calcium FA. It was noted that the mortar continued to gain mechanical strength under normal atmospheric conditions after the initial period of thermal curing.

However, it is worth noting that the strength evolution was higher for mortars with initial curing at ambient temperature (ASN1 and AEA2), exhibiting evolutions of 26 times and 18 times, respectively. In contrast, TSN4 and TEA5 influenced a percentage increase of 11.65% and 0.23% concerning the previous age.

At 63 days, the mortar under the TSN4 condition maintained the highest average compressive strength, reaching 52.2 MPa, while the lowest result was observed for the mortar exposed to the AEA2 curing condition, with 34.89 MPa.

Similarly to the 28-day age, at the age of 63 days, the behavior of samples subjected to curing conditions was comparable, indicating an increase in strength values compared to earlier ages, except ASN1, which showed a

0.91% reduction when compared to the strength value at the age of 28 days. This could be interpreted as a result of some variation in the testing dynamics.

At 91 days, ASN1, AEA2, ASS3, and TSN4 showed a subtle gain in strength in comparison to earlier ages (63 days), with ASS3 presenting the highest percentage increase in strength at 15.40%. However, TEA5 and TSS6 exhibited a reduction of more than 5% in the strength values of the mortars.

In general, an increase in curing temperature is expected to accelerate chemical reactions, improving mechanical properties at early ages (Bing-Hui *et al.*, 2014). At ambient temperature, it is usual to experience a more pronounced gain in strength after 28 days, promoting an improved strength evolution at longer ages, after 92 days (Lee *et al.*, 2019).

In the ANOVA, there was a significant difference in the compressive strength results of all mortars subjected to different curing conditions. Additionally, the Tukey test was conducted to identify homogeneous and heterogeneous results among the mortars. The results of the Tukey test are presented in Table 2.

According to the results of the Tukey test presented in Table 2, at the age of 1 day, the mortar under the TSS6 curing condition shows significantly different results from all other conditions. Meanwhile, the conditions ASN1, AEA2, and ASS3 exhibit non-significant differences among themselves, as do TSN4 and TEA5, which also show non-significant differences between them.

Therefore, it can be inferred that thermal curing is the primary factor for controlling strength at early ages, as expected and reported in the literature (Gómez-Casero *et al.,* 2021). On the other hand, the effect of air exposure and interaction with relative humidity, even though observed between samples ASN1 and AEA2, was not statistically considered relevant. This was unexpected, as in a non-saturated water environment with samples fully exposed to the atmosphere, water evaporation leads to a reduction in alkaline solution and an increase in salt precipitation in the pores (Izquierdo *et al.,* 2010).

Table 3. Statistical Analysis by Turkey Test for Compressive Strength.

	ASN1				AEA2				ASS3				TSN4				TEA5				TSS6			
	1	28	63	91	1	28	63	91	1	28	63	91	1	28	63	91	1	28	63	91	1	28	63	91
ASN1																								
AEA2																								
ASS3																								
TSN4																								
TEA5																								
TSS6																								
Legend:			Significant						Not significant								Not applicable							

Submersion curing does not have a significant effect when the mortar is cured at room temperature. However, it was statistically relevant for mortars with initial thermal curing. This finding aligns with previous literature reports. Immersion curing in water is not advised for low-calcium alkali-activated materials, as it may dissolve the reaction activator and reduce the material's strength development (Provis, 2018).

At 28 days, the TSS6 curing condition showed non-significant differences from ASN1 and ASS3, indicating that the strength gain in the mortar with initial thermal curing but submerged curing has no effect compared to mortars with initial room temperature curing. The ASN1, TSN4, and TEA5 curing conditions also did not show significant differences between them, demonstrating that mortars with initial thermal curing did not exhibit significant differences compared to mortars with room temperature curing and no air exposure. Therefore, at 28 days, the ASN1 mortar has a compressive strength of 38.5 MPa without the energy consumption of thermal curing, making it an environmentally advantageous condition.

The Tukey test results for the age of 63 days indicate that the TSN4 curing condition produces results with significant differences from all other conditions, while ASN1 showed non-significant differences with TEA

and TSS6. The TSN4 mortar showed the highest strength gain in this interval. At 91 days, the TSN4 curing condition shows significant differences from all other conditions, while ASN1 and AEA2 show non-significant differences between them, and ASS3 and TEA5 also exhibit non-significant differences between them.

In the long term, it is noted that the isolation from air exposure and absence of interaction with relative humidity were important factors for the TSN4 mortar. This prevented water loss from the samples, keeping water available during matrix hardening (Criado; Fernández-Jiménez; Palomo, 2010).

4.2 MICROSTRUCTURE ANALYSIS

For the microstructure SEM analysis, three mortar samples were examined under different curing conditions: ASN1, cured at room temperature with the specimen exposed to air and interacting with ambient humidity (Figure 3); TSN4, subjected to 24 hours of thermal curing at 50°C with the specimen fully isolated from air and ambient humidity (Figure 4); and TSS6, exposed to 24 hours of thermal curing at 50°C with the specimen initially exposed to air and subsequently submerged in water (Figure 5).

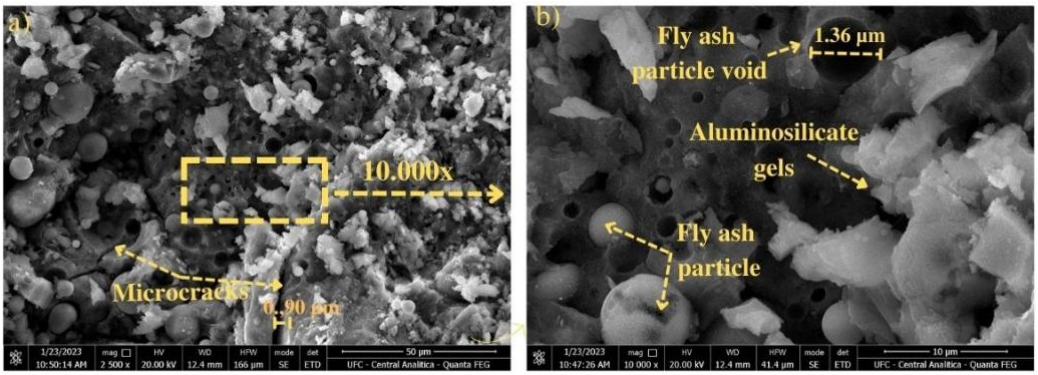

Figure 3. Scanning Electron Microscopy (SEM) of the sample ASN1: a)2500x; b) 10000x.

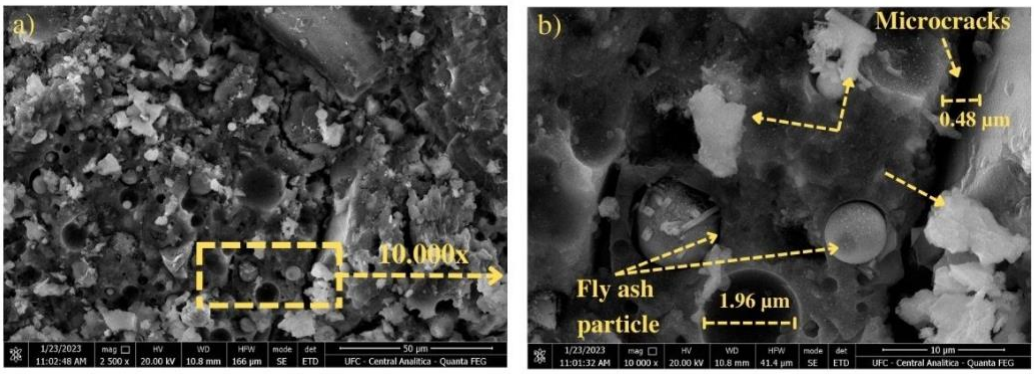

Figure 4. Scanning Electron Microscopy (SEM) of the sample TSN4: a)2500x; b) 10000x.

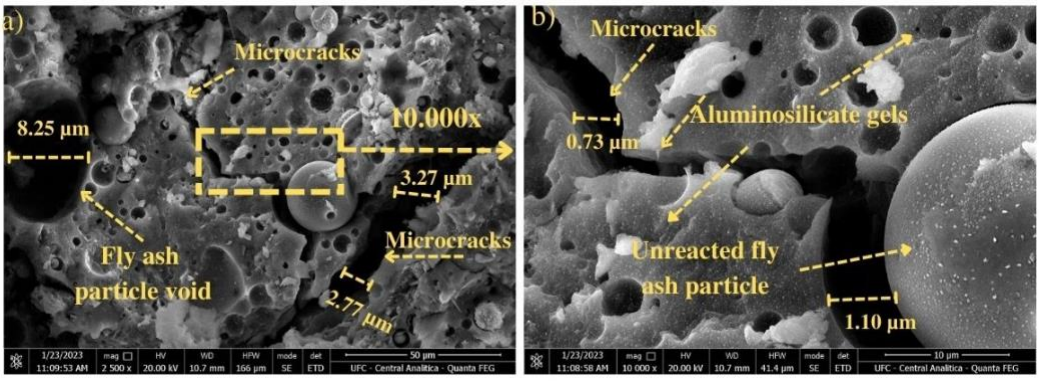

Figure 5. Scanning Electron Microscopy (SEM) of the sample TSS6: a)2500x; b) 10000x.

In all three samples, spherical-shaped fly ash particles are observed, indicating the incomplete dissolution of the precursors. This aspect is commonly found in the literature (Rodríguez *et al.*, 2013).

According to Galiano *et al.*, (2016), the microstructure of alkali-activated materials based on fly ash consists of a relatively dense packing of unreacted particles; an undifferentiated and homogeneous mass surrounding and cementing the particles, i.e., the binding gels; and networks of intergranular and intragranular pores.

The visualization in Figures 3, 4, and 5 allows observing the presence of aluminosilicate gel formation. These gels are responsible for the binding characteristics of AABs. Generally, N-A-S-H type gel is developed for low-calcium systems, C-A-S-H type gel for high-calcium systems, and C-N-A-S-H type gel, which originates from the mixture of both systems forming an intermediate calcium content system (Wan *et al.,* 2020; Provis, 2014; Ismail et al., 2014). Since the AABs used in the mortars consist of fly ash (low calcium content) and BOF slag (high calcium content), the afore mentioned gels may coexist to form the binding microstructure (Costa, 2022).

In all tested samples, the presence of unreacted particles, such as fly ash spheres, is observed in Figures 3, 4, and 5. These unreacted or partially reacted particles are commonly found in AABs (Gebregziabiher *et al.,* 2016; Fernández-Jiménez *et al.,* 2005). The spherical voids identified in the matrix are associated with the hollow spheres of fly ash, called cenospheres. As the reactions occur on the particle's shell, a portion of intraparticle voids is not filled, and their dimensions vary, as seen in Figures 3, 4, and 5. This is a characteristic present in AABs containing fly ash (Bernal & Provis, 2014). Additionally, the presence of microcracks with various thicknesses is noticeable in the microstructure of the cementitious matrix, as observed in Figures 3a, 4b, 5a, and 5b.

In all tested samples, the presence of unreacted particles, such as fly ash spheres, is observed in Figures 3, 4, and 5. These unreacted or partially reacted particles are commonly found in AABs (Gebregziabiher *et al.*, 2016; Fernández-Jiménez *et al.,* 2005). The spherical voids identified in the matrix are associated with the hollow spheres of fly ash, called cenospheres. As the reactions occur on the particle's shell, a portion of intraparticle voids is not filled, and their dimensions vary, as seen in Figures 3, 4, and 5. This is a characteristic present in AABs containing fly ash (Bernal & Provis, 2014). Additionally, the presence of microcracks with various thicknesses is noticeable in the microstructure of the cementitious matrix, as observed in Figures 3a, 4b, 5a, and 5b.

Figure 6 shows the distribution of the void area to complement the microstructure analysis. The images selected for analysis of the distribution of voids show the presence of microcracks in the microstructure of the AABs (Figures 6b, 6c, and 6d). It was found that most of the voids identified had an area of less than 50 μm2, around 86% for the samples in the AEA2 and TSS6 curing conditions and 90% for the samples in the TSN4 curing condition (Figure 6a). According to Galiano *et al.* (2016), the porosity of the materials is affected by thermal activation during curing, and they have lower average pore sizes and higher total pore volumes than those cured at room temperature. In the range of 50 to 100 μm² and in the range of 500 to 2000 μm² the highest concentration of voids is seen for the sample in the TSN4 curing condition, while in the range of 100 to 500 μm², the highest concentration of voids is seen for the AEA2 sample. Beyond 2000 μm², the sample in the TSS6 curing condition had a higher concentration. These last two bands reveal the greater thickness of the microcracks found in the cementitious matrices, indicating that the sample in the TSS6 curing condition had thicker cracks, as can be seen in Figure 5a.

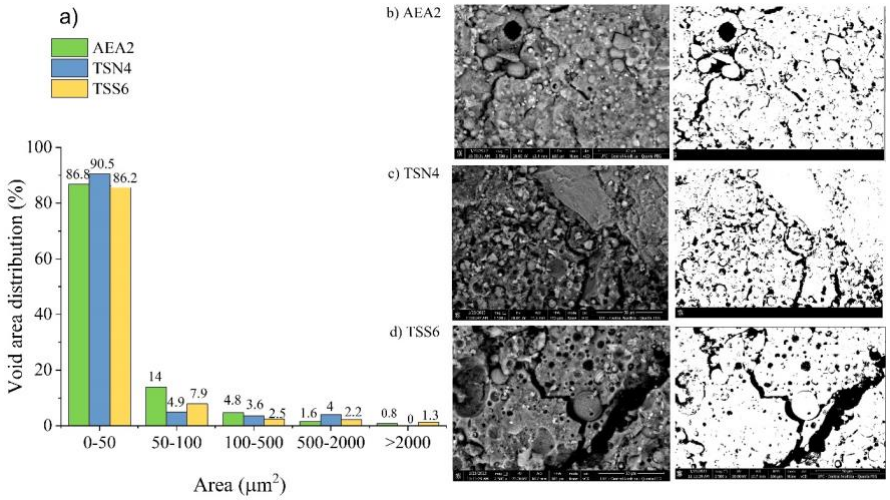

Figure 6. Pore area distribution and processed images in the analysis: a) Void area distribution graphic; b) AEA2; c) TSN4; d) TSS6.

The predominant voids in fly ash-based AABs are composed of large cavities formed by the partial dissolution of original fly ash particles with hollow interiors (cenospheres). These cavities can vary in size, reaching up to 10 μm in diameter (Ma *et al.,* 2013). This aspect can be better visualized in Figures 3, 4, and 5, where some cavities were measured, recording up to 8.25 μm in the TSS6 sample (Figure 5a). Figure 7 presents graphs of void area versus compressive strength for the lower extreme, voids below 50 μm², and the upper extreme, voids above 2000 μm².

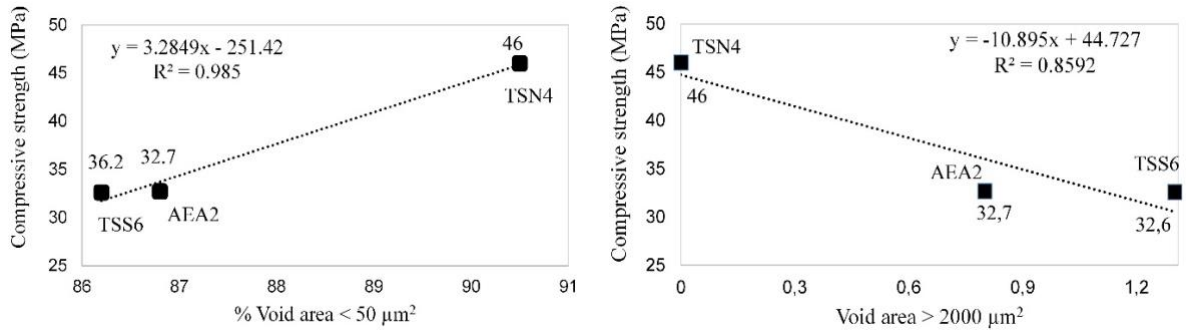

Figure 7. Void Area vs. Compressive Strength: a) % void area < 50 μm²; b) % void area >2000 μm².

In Figure 7, it is possible to identify that voids below 50 μm² do not negatively interfere with compressive strength, as the sample in the TSN4 curing condition had a higher percentage of voids concentrated in this range and achieved the highest compressive strength at 28 days. This phenomenon was also observed by Galiano *et al.* (2016) and Kang *et al.* (2011). Although high porosities were obtained, the reduced dimensions of the voids did not negatively affect the strength. This phenomenon may contribute to the formation of a more uniform and resistant cementitious matrix. It was verified that compressive strength tends to increase with the increase in voids below 50 μm², as per the regression equation model (R^2=0.985) in Figure 7a. Hu *et al.* (2019) also identified a similar behavior in a fly ash-based AABs matrix.

On the other hand, voids above 2000 μm² seem to negatively influence compressive strength, as the higher concentration in this range is observed in the samples in the AEA2 and TSN4 curing conditions, which showed lower resistances. According to the regression equation model (R^2=0.8592) in Figure 7b, compressive strength tends to reduce with the increase in voids larger than 2000 μm². Additionally, as reported by Lloyd *et al.* (2009), larger voids in the matrix may be accessible to the interior of the samples by connecting with capillary pores and affecting the durability of the matrices. The presented models meet the boundary conditions of the present study. The pore structure of fly ash-based geopolymers is highly heterogeneous due to the variable chemical and physical nature of the particles present in the precursors and the complex reaction process that occurs during alkali activation (Provis *et al.,* 2012).

5. Conclusion

This research investigated the influence of different curing conditions on alkali-activated mortar produced with fly ash and basic oxygen furnace (BOF) slag. Mechanical behavior and microstructural aspects were studied. Based on the experimental results, the following conclusions are presented:

- Thermal curing at 50°C for 24 hours accelerated the hardening process and initial strength gain, ensuring higher strengths at advanced ages as well.
- Interaction with ambient water in the submerged condition caused a delay in strength gain compared to samples cured with exposure to air and interaction with the relative humidity of the air, and in the condition without contact and interaction with air humidity.
- Isolating from contact with air and interaction with the relative humidity of the air contributes to better strength results, acting in conjunction with thermal curing and curing at room temperature.
- The microstructure of the mortars consists of aluminosilicate gels, with the likely coexistence of N-A-S-H and C-A-S-H gels, unreacted particles of fly ash and BOF slag, and voids. The voids concentrate in pores with an area below 50 μm², registering more than 85% of the voids in this range. Some microfissures are also present in the matrices, representing areas above 2000 μm², being more expressive in samples cured with exposure to air and interaction with the relative humidity of the air and in the submerged condition, negatively affecting compressive strength.

- In summary, the results of this investigation indicate that the properties of the studied alkali-activated binders can be maximized when produced under the parameters of 50°C for 24 hours, isolated from contact with air, and without interaction with the relative humidity of the air.

ACKNOWLEDGMENTS

The authors would like to thank the National Council for Scientific and Technological Development (CNPq) for supporting project 409236/2022-5.

6. References

American Society for Testing And Materials. ASTM C618 **(**2019)**.** Standard specification for coal fly ash and raw or calcined natural pozzolan for use in concrete.

Araujo, L. (2022). Caracterização de misturas álcali-ativadas à base de cinza volante e escória de aciaria. Dissertação em desenvolvimento (Mestrado em Engenharia Civil), *Programa de Pós-Graduação em Engenharia Civil: Estruturas e Construção Civil*, Universidade Federal do Ceará, Fortaleza, CE, Brasil.

Azevedo, G. S., Strecker, K., de Araújo, A. G.; & da Silva, C. A. (2017). Produção de geopolímeros à base de cinza volante usando soluções ativadoras com diferentes composições de Na2O e Na2SiO3. *Ceramica, 63*(366),143-151. https://doi.org/10.1590/0366-69132017633662078

Bakria, A. M. M. A., Kamarundin, H., Binhussain, M., Nizar, I. K., Zarina, Y., & Rafiza, A. R. (2011). The effect of curing temperature on physical and chemical properties of geopolymers. *Physics Procedia*, 22, 286-291.

Bernal, S. A., & Provis, J. L. (2014). Durability of alkali-activated materials: progress and perspectives. *Journal of the American Ceramic Society,* 97, (4), 997-1008. doi.org/10.1111/jace.12831.

Bing-Hui, M., Zhu, H., Cui., X. M., He, Y., & Gong, S. Y. (2014). Effect of curing temperature on geopolymerization of metakaolin-based geopolymers. *Applied Clay Science,* 99, 144-148. https://doi.org/10.1016/j.clay.2014.06.024

Brazilian Association of Technical Standards. NBR 16372 (2014). Portland cement and other powdered materials – determination of fineness by the air permeability method (Blaine method), Rio de Janeiro.

Brazilian Association of Technical Standards. NBR 16605 (2017). Portland cement and other powdered material – determination of the specific gravity. Rio de Janeiro.

Brazilian Association of Technical Standards. NBR 13276 (2016). Mortars applied on walls and celling – determinations of the consistence index. Rio de Janeiro.

Brazilian Association of Technical Standards. NBR 13279 (2005). Mortars applied on walls and celling – determination of the flexural and compressive strength in the hardened stage. Rio de Janeiro.

Brazilian Association of Technical Standards. NBR 16372 (2015). Portland Cement and the other powdered materials – determination of fineness by the air permeability method (Blaine Method). Rio de Janeiro.

Brazilian Association of Technical Standards. NBR 16973 (2021). Aggregates – determination of material finer than 75µm sieve by washing. Rio de Janeiro.

Brazilian Association of Technical Standards. NBR 17054 (2022). Aggregates – determination of granulometric composition – test method. Rio de Janeiro.

Caetano, P. H. C. (2021). Análise do comportamento no estado fresco e endurecido de pastas álcali ativadas à base de cinzas de combustão de carvão mineral e de escória de aciaria**.** Trabalho de conclusão de curso. Universidade Federal do Ceará. Crateús.

Chindaprasirt, P., Chareerat, T., Hatanaka, S., & Cao, T. (2010). High-strength geopolymer using fine high-calcium fly ash. *J. Mater. Civ. Eng., 23*(3), 264e270.

Chindaprasirt, P., Silva, P., Sagoe-Crentsil, K., & Hanjitsuwan, S. (2010). Effect of SiO_2 and Al_2O_3 on the setting and hardening of high calcium fly ash-based geopolymer systems. *Journal of Materials Science, 47*(12) 4876-4883.

Costa, H.N. (2022). Cimentos álcali-ativados à base de cinzas do carvão mineral e de escórias siderúrgicas. (Tese). Programa de Pós-graduação em Engenharia e Ciência de Materiais, Universidade Federal do Ceará, Fortaleza.

Criado, M., Fernández-Jiménez, A., & Palomo, A. (2010). Alkali activation of fly ash. Part III: Effect of curing conditions on reaction and its graphical description. *Fuel, 89*(11), 3185-3192,

Ding, Y., Shi, C., & Li, N. (2018). Fracture properties of slag/fly ash-based geopolymer concrete cured in ambient temperature. *Construction and Building Materials*, v. 190, p. 787-795.

Duxson, P., Fernández-Jiménez, A., Provis, J. L., Lukey, G. C., Palomo, A., & Van Deventer, J. S. J. (2007). Geopolymer technology: The current state of the art. *Journal of Materials Science, 42*(9), 2917-2933.

Fernández-Jiménez, A., Palomo, A., & Criado, M. (2005). Microstructure development of alkali-activated fly ash cement: A descriptive model. *Cement and Concrete Research, 35*(6), 1204-1209.

Galiano, Y., Fernández-Pereira, C., & Izquierdo, M. (2016). Contributions to the study of porosity in fly ash-based geopolymers. Relationship between degree of reaction, porosity and compressive strength. *Materiales de Construccion, 66*, 324.

Gebregziabiher, B. S., Thomas, R. J., & Peethamparan, S. (2016). Temperature and activator effect on early-age reaction kinetics of alkali-activated slag binders. *Construction and Building Materials*, 113, 783–793.

Gómez-Casero, M. A., Pérez-Villarejo, L, Castro, E., & Eliche-Quesada, D. (2021). Effect of steel slag and curing temperature on the improvement in technological properties of biomass bottom ash based alkali-activated materials. *Construction and Building Materials*, v. 302.

Hu, X., Shi, C., Shi, Z., & Zhang, L. (2019). Compressive strength, pore structure and chloride transport properties of alkali-activated slag/fly ash mortars. *Cement and Concrete Composites*, 104, 103392.

Huseien, G. F., Mirza, J., Ismail, M., & Hussin, M.W. (2016). Influence of different curing temperatures and alkali activators on properties of GBFS geopolymer mortars containing fly ash and palm-oil fuel ash**.** *Construction and Building Materials*, 125, 1229-1240.

Ismail, I., Bernal, S.A., Provis, J.L., Nicolas, R.S., Hamdan, S., & Van Deventer, J.S.J. (2014). Modification of phase evolution in alkali-activated blast furnace slag by the incorporation of fly ash. *Cement and Concrete Composites,* 45, 125-135.

Izquierdo, M., Querol, X., Phillipart, C., Antenucci, D., & Towler, M. (2010). The role of open and closed curing conditions on the leaching properties of fly ash-slag-based geopolymers. *Journal of Hazardous Materials, 176*(1-3), 623-628.

Juenger, M. C. G., Winnefeld, F., Provis, J. L., & Ideker, J. H. (2011). Advances in alternative cementitious binders. *Cement and Concrete Research*, v.41, n. 12, pp. 1232-1243.

Kang, H. J., Ryu, G.S., Koh, G.T., Kang, S.T., & Park, J. J. (2011). Relationship between microscopic structures and compressive strength of alkali-activated fly ash mortar. *Key Engineering Materials,* 452-453, 737-740.

Komljenović, M., Baščarević, Z., & Bradić, V. (2010). Mechanical and microstructural properties of alkali-activated fly ash geopolymers. *Journal of Hazardous Materials, 181*(1-3), 35-42.

Langaro, E. A**. (**2016). Cimento álcali ativado a partir da valorização da escória de alto forno a carvão vegetal**.** Dissertação (Mestrado em Engenharia Civil), Programa de Pós-Graduação em Engenharia Civil, Universidade Tecnológica Federal do Paraná.

Lee, W. H., Wang, J. H., Ding, Y. C., & Cheng, T. W. (2019). A study on the characteristics and microstructures of GGBS/FA based geopolymer paste and concrete. *Constr. Build. Mater.,* 211, 807-813, doi.org/10.1016/j.conbuildmat.2019.03.291.

Lloyd R.R., Provis J.L., Smeaton K.J., & Van Deventer, J.S.J. (2009). Spatial distribution of pores in fly ash-based inorganic polymer gels visualised by Wood's metal intrusion. *Micropor Mesopor Mater, 126*(1-2), 32-9.

MA, Y., HU, J., & YE, G. (2013). The pore structure and permeability of alkali activated fly ash. *Fuel*, 104, 771-780.

Mian, A., Bending, M., Piazzessi, G., Manente, G., Lazzaretto, A., & Maréchal, F. (2013). Energy integration in the cement industry. *Computer Aided Chemical Engineering*, 32, 349-354.

Monteiro, P. J. M.; Miller, S. A.; Horvath, A. (2017). Towards sustainable concrete. *Nature Materials, 16*(7) 698-699.

National Road Department. DNER ME 194 (1998). Aggregates – Determination of the specific mass of fine aggregates using the Chapman bottle. Rio de Janeiro.

Nath, S. K., Maitra, S., Mukherjee, S., & Kumar, S. (2016). Microstructural and morphological evolution of fly ash based geopolymers. *Construction and Building Materials*, 111, 758-765.

Provis, J. L (2018). Alkali-activated materials. *Cement and Concrete Research*, 114, 40-48.

Provis, J. L., Myers, R. J., White, C.E., Rose, V., & Van Deventer, J.S.J. (2012). X-ray microtomography shows pore structure and tortuosity in alkali-activated binders. *Cement and Concrete Research, 42*(6), 855-864.

Provis, J. L. (2014). Geopolymers and other alkali activated materials: Why, how, and what? *Materials and Structures, 47*(1-2), 11-25.

Provis, J. L., & Van Daventer, J. S. J. (2014). Alkali-Activated Materials: State-of-the-Art Report, RILEM TC 224-AAM. Springer.

Rai, B., Roy, L. B., & Rajjak, M. (2018). A statistical investigation of different parameters influencing compressive strength of fly ash induced geopolymer concrete. *Structural Concrete, 19*(5), 1268-1279.

Rodríguez, E. D., Bernal, S.A., Provis, J.L, Paya, J., Monzo, J., & Borrachero, M.V. (2013). Effect of nanosilica-based activators on the performance of an alkali-activated fly ash binder. *Cement and Concrete Composites, 35*(1), 1-11.

Sathonsaowaphak, A., Chindaprasirt, P., & Pimraksa, K. (2009). Workability and strength of lignite bottom ash geopolymer mortar. *Journal of Hazardous Materials, 168* (1), 44-50.

Silva, R. V., Brito, J., Lynn, C.J., & Dhir, R.K. (2017). Use of municipal solid waste incineration bottom ashes in alkali-activated materials, ceramics and granular applications: A review. *Waste Management, 68,* 207-220.

Sindicato Nacional das Indústrias de Cimento (2022). Relatório Anual 2022. Disponível em: https://snic.org.br/assets/pdf/relatorio_anual/rel_anual_2022.pdf

Soutsos, M., Boyle, A. P., Vinai, R., Hadjierakleous, A., & Barnett, S. J. (2016). Factors influencing the compressive strength of fly ash based geopolymers. *Construction and Building Materials*, 110, 355-368.

Sun, Y., Zhang, S., Rahul, A. V., Tao, Y., Van Bockstaele, F., Dewettinck, K., Ye, G., & De Schutter, G. (2022). Rheology of alkali-activated slag pastes: New insight from microstructural investigations by cryo-SEM. *Cement and Concrete Research*, 157.

Targino. D. L., Araujo, L.B., Paiva, A., Costa, H.N., & Cabral, A.E.B. (2024). Concretos sustentáveis com aglomerantes geopoliméricos e agregados de escória de aciaria BSSF: caracterização mecânica e análise de impacto ambiental. Trabalho em desenvolvimento (Mestrado em Engenharia Civil), Programa de Pós-Graduação em Engenharia Civil: Estruturas e Construção Civil, Universidade Federal do Ceará, Fortaleza.

Thomas, R. J., & Peethamparan, S. (2017). Stepwise regression modeling for compressive strength of alkali-activated concrete. *Construction and Building Materials*, 141, 315-324.

Wan, H., Yuan, L., & Zhang, Y. (2020). Insight Into the Leaching of Sodium Alumino-Silicate Hydrate (N-A-S-H) Gel: A Molecular Dynamics Study. *Frontiers in Materials,* 7, 1-11.

Zhang, P., Zheng, Y., Wang, K., & Zhang, J. (2018). A review on properties of fresh and hardened geopolymer mortar. Composites Part B: Engineering, 152, 79-95.